



Light emitting devices based on nanocrystalline-silicon multilayer structure

M. Wang^{a,*}, A. Anopchenko^a, A. Marconi^a, E. Moser^a, S. Prezioso^a, L. Pavesi^a,
G. Pucker^b, P. Bellutti^b, L. Vanzetti^c

^a Laboratorio di Nanoscienze, Dipartimento di Fisica, Università di Trento, Via Sommarive 14, 38100 Povo, Trento, Italy

^b Microtechnologies Laboratory, Fondazione Bruno Kessler, Via Sommarive 18, 38100 Povo, Trento, Italy

^c Materials and Analytical Methods Laboratory for Biosensors and Bioelectronics, Fondazione Bruno Kessler, Via Sommarive 18, 38100 Povo, Trento, Italy

ARTICLE INFO

Available online 13 August 2008

PACS:

73.21.Ac
78.67.Bf
78.67.Pt
78.55.Ap
81.15.Gh
85.60.Jb

Keywords:

Silicon nanocrystals
Multilayer structure
PECVD
Ellipsometry
Photoluminescence
Light emitting devices

ABSTRACT

In this paper we report the visible–near-infrared light emission properties of nanocrystalline silicon (nc-Si) light emitting devices (LEDs) based on nc-Si/SiO₂ multilayer structures. Multilayer structures of silicon-rich oxide (SRO) and SiO₂ were grown by plasma enhanced chemical vapor deposition (PECVD) and studied by transmission electron microscopy (TEM) and ellipsometry. A higher nc-Si density in the multilayer samples than in the homogeneous sample was found by comparing photoluminescence (PL) intensities. The PL band located in the near-infrared region can be tuned by the size of nc-Si, which in the multilayer sample is controlled by the thickness of the SRO layer. The multilayer LED shows a much larger current density under low applied voltages than the LED based on a single thick layer. The significant lower driving voltage and enhanced light emission intensity suggest higher power efficiency in multilayer LED. It is believed that the improvement of the LED characteristics is due to the higher nc-Si density caused by the multilayer structure.

© 2008 Elsevier B.V. All rights reserved.

1. Introduction

As the critical dimension of the microelectronics industry is shrinking down to a few nm, standard interconnection scheme shows their limit. Optical interconnection has been proposed for more than two decades [1]. Optical interconnections have several advantages such as larger band width, less signal delay and lower power consumption, but this architecture needs for a silicon-compatible light source that can be integrated into microelectronic devices [2]. The observation of the light emitting property in porous silicon was promising [3]. Following porous silicon, silicon-rich oxide (SRO) [4], amorphous silicon/silicon dioxide superlattice [5], SRO/silicon dioxide superlattice [6], as well as silicon-rich nitride [7] and superlattice [8] have been widely studied in order to optimize the light emission property as well as to clarify the correlation between silicon nanocrystals (nc-Si) and light emission.

Among all the techniques used to produce passivated nc-Si [9,10], layer-by-layer deposition [5,6] of amorphous silicon or SRO and SiO₂ is a promising approach, offering a better control over the density of nc-Si as well as their size distribution. It has also

been reported that the self-organization of the nc-Si in the layer-growth direction could be promoted in nc-Si superlattice structures, through which resonant tunneling occurs and facilitates the carrier transport perpendicular to the layers [11,12]. Although there are a number of results of structural and photoluminescence (PL) studies, electroluminescence (EL) devices and carriers transport of nc-Si superlattice structures are not well understood yet [13,14].

As for device application, it is essential to understand the carrier transport inside the nc-Si systems. When separated by a relatively thick oxide barrier, carriers can be injected into nc-Si by Fowler–Nordheim tunneling [15,16]. This energetic tunneling process degrades the oxide and causes reliability problem to the devices. However, considerable carrier injection is necessary to achieve enough optical output from nc-Si light emitting diode (LED). Therefore, reducing the barrier thickness to a value where direct tunneling occurs could be a solution to decreasing the driving voltage, thus making more reliable devices.

In this paper, we will present plasma enhanced chemical vapor deposition (PECVD)-grown nc-Si/SiO₂ multilayer LEDs. Structural information on the multilayer structure measured by ellipsometry will be shown and compared with transmission electron microscopy (TEM) images. PL and EL under direct current injection will be discussed.

* Corresponding author. Permanent address: State Key Laboratory of Silicon Materials, Zhejiang University, Hangzhou 310027, People's Republic of China.
E-mail address: wang@science.unitn.it (M. Wang).

2. Experimental

The SRO/SiO₂ multilayer was deposited by PECVD on <100> p-type silicon (8–20 Ω cm) substrates. Before deposition an HF dip was applied to all substrates to remove the native oxide. The deposition procedure started with SiO₂ deposition. After that, the PECVD chamber was pumped down, and filled with a new ratio of SiH₄ and N₂O for SRO deposition. The SRO layer was grown after gas stabilization. The alternative growth of SiO₂ and SRO was repeated for 5 periods and ended with an additional SiO₂ deposition. Two samples with 3 or 4 nm (nominal thickness) SRO layers are discussed in this work and their structures are studied by variable-angle spectroscopic ellipsometry, results of which are reported in Table 1. The total thickness of the structure varies from 20 to 30 nm depending on the layer thickness.

The atomic composition of the films was obtained by X-ray photoelectron spectroscopy. The SRO layer in the multilayer stack is composed of 52 at% of silicon, 44 at% of oxygen and 4 at% of nitrogen. Assuming the composition of SiO₂ as 33 at% silicon and 67 at% oxygen, the average silicon content in the multilayer sample is 45 at% for the sample with (SRO 4 nm/SiO₂ 2 nm) and 5 periods, while it is 44 at% for the sample with (SRO 3 nm/SiO₂ 2 nm) and 5 periods.

After the multilayer deposition, 100 nm n+poly-Si was deposited on the multilayer structure as the semi-transparent gate electrode. Wet oxidation was then performed at 1150 °C for 30 min to grow both 500-nm-thick field oxide for device isolation and nc-Si in the gate dielectric. Different geometries were used for metallization: a circular geometry with a ring-shaped metal line for emission studies (LED) and disk geometry entirely covered by the metal contact for electrical studies (capacitor). In the LED geometry, the poly-Si is covered by an anti-reflective coating formed by a 50-nm-thick Si₃N₄ layer and a 120-nm-thick SiO₂ layer to improve light extraction. The anti-reflective coating is used to optimize the transmittance (*T*) in a wide spectral range: *T* is larger than 50 at% at 500 nm and larger than 85% from 650 nm onwards. Fig. 1 reports the schematic cross-section, top view of the device and the cross-sectional TEM image of the nc-Si/SiO₂ multilayer. The periodic structure is revealed as alternating white and gray stripes, which are SiO₂ layers and nc-Si layers, respectively. The multilayer LED characteristics will be compared with the best characteristics of a single active layer LED [17]. The single active layer is formed by a homogeneous SRO layer of 49 ± 2 nm thickness and with the following composition: 44 at% of silicon, 50 at% of oxygen and 6 at% of nitrogen. Thus, the average silicon content in this homogeneous layer sample is very close to that of the multilayer LED.

The PL measurement was performed on a dedicated area on the wafer having identical active material as the devices. PL spectra were excited by the 488 nm line (~15 W/cm²) and were recorded by a monochromator with a visible photomultiplier tube (PMT). The current–voltage (*I*–*V*) characteristics of the devices were obtained using an Agilent 4156C precision semiconductor parameter analyzer. The EL was collected with a Spectra-Pro 2300i

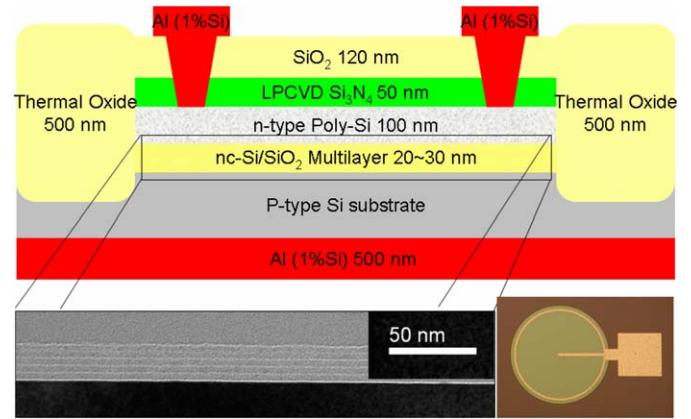


Fig. 1. LED schematic cross-section (top), top view of the LED (bottom right) and TEM image (bottom left) of the nc-Si/SiO₂ multilayer (annealed structure of SRO 4 nm/SiO₂ 2 nm, 5 periods).

monochromator coupled with a nitrogen-cooled CCD camera. The total EL emitted power was measured with a large-area PIN photodiode (UDT PIN-10DF), whose output current signal was measured by a Keithley 6485 picoamperometer. The photodiode was placed within a few millimeters above the device. No corrections for the collection geometry were taken into account. All the measurements were performed at room temperature.

3. Results and discussion

3.1. Ellipsometry and photoluminescence studies

The layer thickness of the as-deposited SRO/SiO₂ multilayer structure shown in Table 1 was obtained from ellipsometry measured with three angles (50°, 60° and 70°) in the spectral range from 300 to 850 nm. The refractive index and extinction coefficient versus wavelength of SRO and SiO₂ materials were previously determined from single layers. By modeling the multilayer structure with these predetermined parameters, the layer thickness of SRO and SiO₂ in the multilayer was obtained as well as the total thickness of structures. One should note that the actual found layer thickness is smaller than the nominal value estimated from the deposition rate. The origin of this difference is in the delay of plasma ignition. After annealing, nc-Si grow from SRO layer. The refractive index and extinction coefficient of the SRO layer change. The same model cannot be applied for the annealed samples. As an alternative, TEM image of annealed structure is shown in Fig. 1. One should note that the nc-Si layer is thicker than the initial SRO layer when the SRO layer thickness in Table 1 is compared with the TEM image. The thickness difference indicates that during high-temperature annealing Si atoms diffuse between the layer, which, as a result, roughens the layer interface and reduces the SiO₂ layer thickness.

In Fig. 2(a), the PL spectra of multilayer structures are compared with the corresponding one of SRO and SiO₂ single layer. PECVD SiO₂ film only shows weak luminescence around 630 nm, which can be assigned to the non-bridging oxygen hole center [18]. Since all the spectra were collected from the area covered by poly-Si, the absence of infrared luminescence in the SiO₂ sample excludes the presence of poly-Si light emission in this spectra range. The spectrum of the SRO single layer shows a typical nc-Si emission band around 800 nm. Taking into account literature results [6,19], the average nc-Si size should be close to 2 nm. For the multilayer structures with the initial SRO layer thicker than 2 nm, the PL bands red-shift into near infrared and

Table 1

Layer thicknesses of the as-deposited SRO/SiO₂ multilayer structures obtained from ellipsometry, total thickness of the structures is calculated from the layer thickness and the number of the layers (5 layers of SRO and 6 layers of SiO₂)

Nominal multilayer thickness	SRO layer thickness (nm)	SiO ₂ layer thickness (nm)	Total thickness (nm)
SRO 4 nm/SiO ₂ 2 nm	3.12 ± 0.02	1.52 ± 0.03	24.72 ± 0.28
SRO 3 nm/SiO ₂ 2 nm	1.94 ± 0.02	1.84 ± 0.03	20.74 ± 0.28

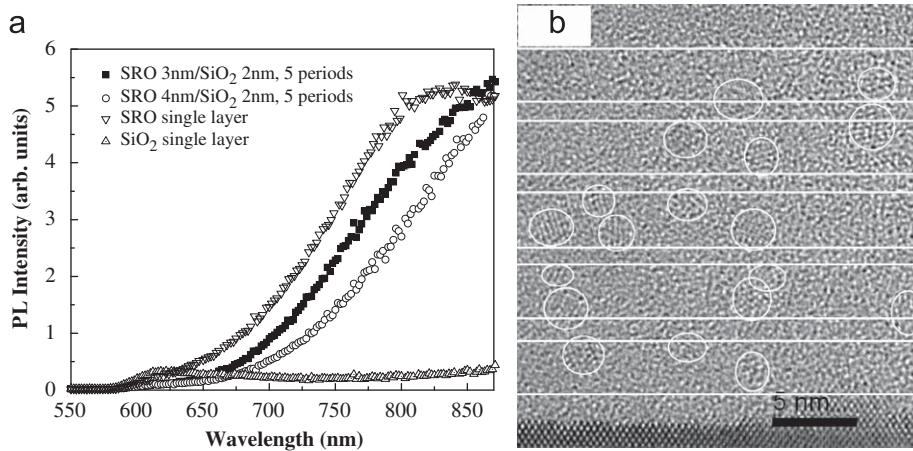


Fig. 2. (a) Photoluminescence spectra of the nc-Si/SiO₂ multilayers (Ar laser line at 488 nm, ~15 W/cm²). Single layer of SRO and SiO₂ is shown for comparison. The thickness of the SRO single layer is 49 ± 2 nm. The SRO single layer was annealed at 1050 °C for 1 h. The total thickness of the multilayer structure is between 20 and 30 nm (see Table 1), and annealed at 1150 °C for 30 min. (b) High-resolution TEM image of multilayer SRO_4 nm/SiO₂_2 nm is shown. The average size of silicon nanocrystals is about 2.5 nm. For clarity, the visible nanocrystals are highlighted by circles and the layers are indicated by lines.

their maxima do not appear in the spectra range of Fig. 2. Moreover, the PL spectrum of the SRO 4 nm/SiO₂ 2 nm multilayer is further red-shifted than the one of the SRO 3 nm/SiO₂ 2 nm multilayer. According to quantum confinement effect, the red-shift indicates larger nc-Si in thicker SRO layer. The PL intensity of the multilayer sample is comparable with the intensity of the single-layer sample while the thickness of the single layer is about twice of that of the multilayer. This suggests a higher nc-Si density in the multilayer sample than in the single-layer one. In Fig. 2(b), the high-resolution TEM image of the SRO_4 nm/SiO₂_2 nm multilayer sample is shown. The average size of nc-Si is about 2.5 nm. Note that only crystals having the right orientation with respect to the incident electron beam can be seen by their lattice images. Most of the nanocrystals are contained inside the SRO layers while some of them grew over into the SiO₂ layer. This also should be attributed to the silicon diffusion between the layers that is enhanced by a high annealing temperature. Further optimization of the annealing procedure or material engineering is necessary to control the growth of nc-Si.

3.2. Electro-optical characteristics under direct current (DC)

To compare the I - V characteristics of devices with a single layer and a multilayer, the gate current density is plotted against the applied electric field, in Fig. 3. Only the forward bias branch in the I - V curves is shown (applying negative voltage on the n-type poly gate and grounding the substrate). The measured electric field was calculated from the applied gate voltage corrected for the trapped charge. The trapped charge (the net positive charge) causes the horizontal shift of the I - V characteristics. The total thickness of the structure (shown in Table 1) is used in the calculation of the electric field.

In Fig. 3, two distinct regions can be observed in the log-log plot, which are more evident in the multilayer devices. The current density shows a weak increase in the low electric field region (for multilayer devices, it is up to 0.5 MV/cm) and increases much faster in the region of high fields. The device with SRO 3 nm/SiO₂ 2 nm structure shows a current density two orders of magnitude larger than that of the single-layer LED at the low electric fields. By increasing the field, the difference of the current density between the single layer and the multilayer becomes smaller. Taking into account the same average silicon content, the device with SRO 3 nm/SiO₂ 2 nm structure has the same high-field

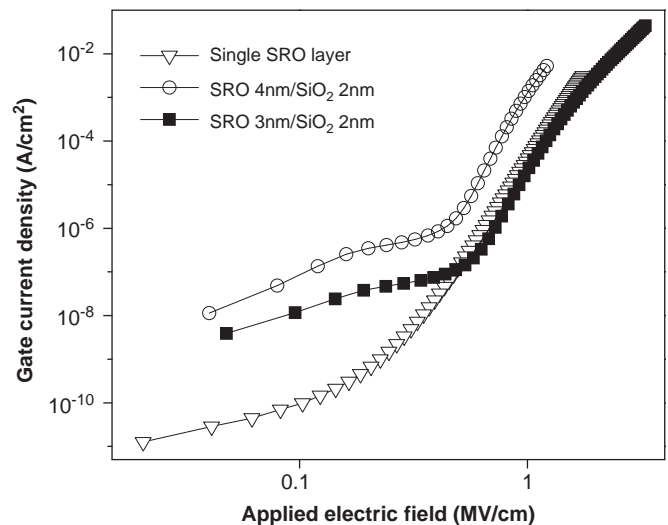


Fig. 3. Gate current density as a function of applied electric field. Two distinct regions can be observed in this log-log plot. Multilayer devices show much higher current density in the low electric field region. The multilayer SRO 3 nm/SiO₂ 2 nm has the same average silicon content as the single layer and lower silicon content than the SRO 4 nm/SiO₂ 2 nm.

I - V characteristic as the single-layer LED. In the whole field range, the device with the SRO 4 nm/SiO₂ 2 nm structure shows higher current density than other devices. This observation is consistent with the difference in the silicon content. The device with the thicker SRO layer has higher silicon content and, possibly, larger nc-Si size, which leads to the higher conductivity. We believe that the enhanced currents at the low electric fields in the multilayer device originates from the direct charge tunneling from the substrate into the nc-Si and then into the gate. In the multilayer structure, a high nanocrystal density is expected, i.e. nc-Si are closer and the oxide thickness between them is reduced, which facilitates the carrier transport.

EL spectra collected from the single-layer and multilayer LEDs are shown in Fig. 4. The spectra from the SRO 4 nm/SiO₂ 2 nm multilayer and the SRO single-layer devices peak at about the same wavelength, 920 nm under low (10 μ A) and high (100 μ A) injected current. At the same injected current of 10 μ A, the EL peak intensity almost doubles in multilayer devices, while the

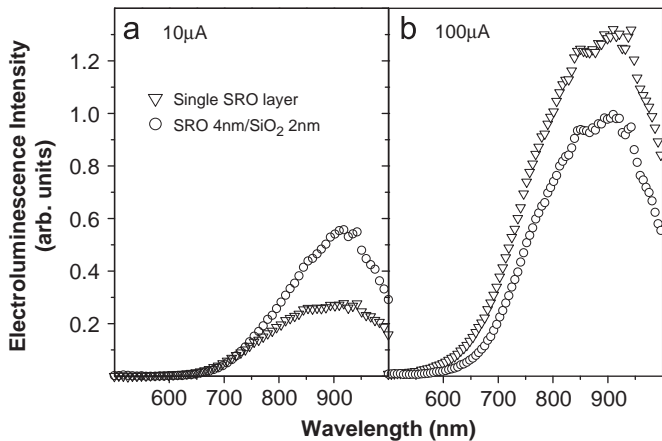


Fig. 4. Electroluminescence spectra at the injection current of 10 μA (a) and 100 μA (b). (a) The gate voltage is 13.5 and 3.4 V for the single-layer LED and multilayer LED (SRO 4 nm/SiO₂ 2 nm), respectively. (b) The gate voltage is 18.4 and 5.2 V for the single-layer LED and multilayer LED (SRO 4 nm/SiO₂ 2 nm), respectively.

applied gate voltage is four times smaller than the single thick-layer LED (Fig. 4a). Although the decrease in the applied voltage is partially due to the thickness difference, higher EL intensity at the same injection level still indicates a more efficient electrical excitation in the multilayer. The power efficiency measured at 10 μA is 2×10^{-7} for the single-layer device and 10^{-6} for the multilayer device. However, at 100 μA the EL emission is larger in the single-layer LED (Fig. 4b), which points to a change in the light emission mechanism at this high applied bias (18.4 V). We have shown [17] that the EL emission at high voltage originates from hot-electron injection and impact ionization, and it is more sensitive to the applied voltage rather than injection current. Moreover, the efficiency of both LEDs decreases as the injected current increases. Under a high injection level, non-radiative recombination processes, such as the Auger process [20], become prominent; at the same time the electric stress-induced oxide defects could be multiplied under a high voltage. Both of them can reduce EL efficiency.

Under low applied voltage, the carriers are injected mostly through the tunneling process [21]. As discussed in Fig. 3, the current is increased probably due to the contribution of the direct tunneling component. Therefore, it is reasonable to believe that this direct tunneling component increases the EL efficiency at an applied bias as low as 3.4 V in the multilayer devices.

4. Conclusions

The structural and electro-optical properties of nc-Si/SiO₂ multilayer LEDs have been studied. The as-deposited and annealed multilayer structures grown by PECVD were examined by ellipsometry and TEM. Higher nc-Si density was found for the

multilayer structure by comparing the PL intensity of multilayer with a thick single layer under similar average silicon content. The PL band located in the near-infrared region can be tuned by the size of nc-Si depending on the thickness of the SRO layer. The carrier transport and EL are dominated by different mechanisms under low and high electric fields. At high fields, the EL originates from impact ionization, showing a low efficiency. While at low fields, the injected current is increased by two orders of magnitude due to the higher nc-Si density in the multilayer devices. For the multilayer LED, the EL intensity is increased even under low bias (3.4 V), showing higher power efficiency. This phenomenon might suggest bipolar injection of electron and hole into nc-Si through the direct tunneling under low bias. Further study is under way to understand the transport mechanism and to improve the multilayer LED.

Acknowledgements

We acknowledge support of Intel Corporation and of EC through the Projects NMP4-CT-2004-505285 Seminano and ICT-FP7-224312 HELIOS.

References

- [1] J.W. Goodman, F.I. Leonberger, S.-Y. Kung, R.A. Athale, Proc. IEEE 72 (1984) 850.
- [2] S. Ossicini, L. Pavesi, F. Priolo, Light Emitting Silicon for Microphotonics, Springer, Heidelberg, Berlin, 2003.
- [3] A.G. Cullis, L.T. Canham, P.D.J. Calcott, J. Appl. Phys. 82 (1997) 909.
- [4] H. Takagi, H. Ogawa, Y. Yamazaki, A. Ishizaki, T. Nakagiri, Appl. Phys. Lett. 56 (1990) 2379.
- [5] Z.H. Lu, D.J. Lockwood, J.M. Baribeau, Nature 378 (1995) 258.
- [6] M. Zacharias, J. Heitmann, R. Scholz, U. Kahler, M. Schmidt, J. Blasing, Appl. Phys. Lett. 80 (2002) 661.
- [7] N.-M. Park, C.-J. Choi, T.-Y. Seong, S.-J. Park, Phys. Rev. Lett. 86 (2001) 1355.
- [8] K. Chen, X. Huang, J. Xu, D. Feng, Appl. Phys. Lett. 61 (1992) 2069.
- [9] S. Guha, M.D. Pace, D.N. Dunn, I.L. Singer, Appl. Phys. Lett. 70 (1997) 1207.
- [10] V.G. Baru, A.P. Chernushich, V.A. Luzanov, G.V. Stepanov, L. Yu, Zakharov, K.P. O'Donnell, I.V. Bradley, N.N. Melnik, Appl. Phys. Lett. 69 (1996) 4148.
- [11] D.J. Lockwood, L. Tsybeskov, in: Encyclopedia of Nanoscience and Nanotechnology, vol. 6, American Scientific Publishers, 2004, p. 477.
- [12] L. Tsybeskov, G.F. Grom, R. Krishnan, L. Montes, P.M. Fauchet, D. Kovalev, J. Diener, V. Timoshenko, F. Koch, J.P. McCaffrey, J.-M. Baribeau, G.I. Sproule, D.J. Lockwood, Y.M. Niquet, C. Delerue, G. Allan, Europhys. Lett. 55 (2001) 552.
- [13] R. Rölver, S. Brünninghoff, M. Först, B. Spangenberg, H. Kurz, J. Vac. Sci. Technol. B 23 (2005) 3214.
- [14] Q. Zhang, A. Filios, C. Lofgren, R. Tsu, Physica E 8 (2000) 365.
- [15] D.J. Dimaria, E.J. Pakulis, D.W. Dong, T.S. Kuan, F.L. Pesavento, T.N. Theis, J.A. Cutro, J. Appl. Phys. 56 (1984) 401.
- [16] G. Franzò, A. Irrera, E.C. Moreira, M. Miritello, F. Iacona, D. Sanfilippo, G. Di Stefano, P.G. Fallica, F. Priolo, Appl. Phys. A 74 (2002) 1.
- [17] S. Prezioso, A. Anopchenko, Z. Gaburro, L. Pavesi, G. Pucker, L. Vanzetti, P. Bellutti, J. Appl. Phys. 104 (2008), to be published.
- [18] G.-R. Lin, C.-J. Lin, C.-K. Lin, L.-J. Chou, Y.-L. Chueh, J. Appl. Phys. 97 (2005) 094306.
- [19] F. Iacona, G. Franzò, C. Spinella, J. Appl. Phys. 87 (2000) 1295.
- [20] A. Irrera, F. Iacona, I. Crupi, C.D. Presti, G. Franzò, C. Bongiorno, D. Sanfilippo, G.D. Stefano, A. Piana, P.G. Fallica, A. Canino, F. Priolo, Nanotechnology 17 (2006) 1428.
- [21] B. De Salvo, G. Ghibaudo, P. Luthereau, T. Baron, B. Guillaumot, G. Reimbold, Solid-State Electron. 45 (2001) 1513.